JOURNAL OF GUIDANCE, CONTROL, AND DYNAMICS
Vol. 30, No. 4, July–August 2007

Multi-Input/Multi-Output Adaptive Output Feedback Control Design for Aeroelastic Vibration Suppression

K. K. Reddy*
University of Central Florida, Orlando, Florida 32816-2362
J. Chen†
University of Michigan, Flint, Michigan 48502
A. Behal‡
University of Central Florida, Orlando, Florida 32816-2362
and
P. Marzocca§
Clarkson University, Potsdam, New York 13699

DOI: 10.2514/1.27684

Via the use of leading- and trailing-edge control surface actuation, an adaptive output feedback controller is designed for suppressing aeroelastic vibrations on a nonlinear wing section. Although a single flap under adaptive control can suppress vibrations, the response rate is limited by the system zero dynamics. Under the restriction that only pitching and plunging variables are available for measurement but their rates are not, the proposed algorithm addresses the problem of designing a singularity-free adaptive output feedback controller when the control inputs are coupled via an input gain matrix for which the parameters are uncertain. The stability result achieved is global asymptotic tracking. Simulation results demonstrate the efficacy of the multi-input/multi-output control toward suppressing flutter and limit-cycle oscillations, as well as reducing the vibrational level in the subcritical flight-speed range. Pertinent conclusions are outlined.

Nomenclature

a	=	nondimensional distance from midchord to the elastic axis
b	=	semichord
$C_{l\alpha}$, $C_{m\alpha}$	=	rate of change of lift and moment, respectively, with respect to the angle of attack
c_h, c_α	=	structural damping coefficients in the plunge and pitch axes, respectively
I_α	=	inertia of the wing section about the elastic axis
k_h, k_α	=	structural spring stiffness in the plunge and pitch axes, respectively
L, M	=	aerodynamic lift and moment
m_w, m_T	=	mass of wing, pitch-plunge system
s	=	wing-section span
U	=	freestream velocity
x_α	=	dimensionless distance from the elastic axis to midchord
α, h, β, γ	=	pitching, plunging, trailing-edge-flap, leading-edge-flap displacements, respectively
ρ	=	air density

Received 6 September 2006; revision received 16 January 2007; accepted for publication 12 February 2007.

*Graduate Student, School of Electrical Engineering and Computer Science.
†Post-Doctoral Fellow, Naval Architecture and Marine Engineering.
‡Assistant Professor, School of Electrical Engineering and Computer Science and NanoScience Technology Center; abehal@mail.ucf.edu.
§Assistant Professor, Mechanical and Aeronautical Engineering; pmarzocc@clarkson.edu.

I. Introduction

AEROELASTICITY has been and continues to be an extremely important concern in aircraft design [1]. Dynamic aeroelastic effects such as flutter and limit-cycle oscillations (LCO) may provide critical constraints on the flight vehicle performance. Although aeroelastic instabilities can be suppressed by increasing the stiffness of the wing, the byproduct of adding weight does decrease the overall performance of the flight vehicle. A possible solution to this problem is via controlling the aeroelastic behavior by feedback to control surfaces. A review of active control methods, wind-tunnel experiments, and flight experiences associated with feedback control and aeroelasticity is presented in [2].

Currently, most aeroelasticity considerations are routinely addressed by assuming linear structural and linear aerodynamic models. However, within the last few years, there has been a significant increase in advancing methods to consider nonlinear aeroelasticity, especially, to account for the presence of softening or hardening structural-stiffness effects and aerodynamic nonlinearities in the transonic or stall region. Dowell et al. [3] shed some light on the importance of considering nonlinearities in the aeroelastic analysis. Among the various nonlinearities, hardening structural nonlinearities (such as those due to the presence of free play) give rise to nonlinear stiffness, especially in torsion. Many times, this type of nonlinearity can have a pronounced effect on control surface flutter. It usually leads to a limited-amplitude aeroelastic behavior, which is not catastrophic but may cause fatigue problems [4–8].

Research focusing on the aeroelastic active control and flutter suppression of aeroelastic systems with structural nonlinearity is increasing. A number of recent contributions related to the active control of aircraft wings are discussed at length in [9–11]. For examples of studies that examine control of structurally nonlinear aeroelastic systems, the reader is referred to [12–16]. In particular, several control strategies were examined for a typical wing section with a single control surface and were verified experimentally [12–15]. Using nonlinear control theory, feedback linearization techniques as well as robust and adaptive controllers were proposed in [17–23]. In most of the aforementioned methods, the pitching degree of freedom α is chosen as the primary output variable to

regulate to the origin. Initially, an adaptive cancellation of the nonlinearities introduced by the torsional stiffness leads to a feedback linearized system; subsequently, a second control step aims to enhance the aeroelastic response via conventional linear methods such as a linear quadratic regulator or pole placement. The eventual controller designed in these references is full-state feedback. In [23], an adaptive control strategy was implemented using only the feedback for the pitching variable, its performance was demonstrated in subcritical flight-speed range toward suppressing flutter and LCOs, as well as reducing the aeroelastic response in the subcritical flight-speed regime.

A problem due to feedback linearization with these single-input adaptive controllers is that the aeroelastic response is limited by the system zeros that end up in the closed-loop system characteristic polynomial. Another practical problem is that adaptive control works well with velocities limited up to approximately 23% greater than the velocity of LCO onset. In [24], a better way of improving the performance of the adaptive scheme via an extension to a wing section with two control surfaces was proposed. The scheme proposed was adaptive and used full-state feedback. However, the uncertainty in the coupling between the control inputs was not taken into account; instead, a simple inversion of a (nonsingular and nonsymmetric) nominal input gain matrix was used to decouple the control inputs. This problem was solved via a full-state feedback adaptive controller of a 2-D wing with leading-edge (LECS) and trailing-edge (TECS) control surfaces proposed in [25]; this approach was shown to have better dynamic performance than a single control surface. For details on the backstepping design for multivariable systems using symmetric-diagonal-upper-triangular (SDU) factorization and application to LECS/TECS, we refer the reader to [26,27].

In this paper, we achieve adaptive global asymptotic vibration suppression as similarly done in [25], but by using only output feedback (i.e., using the measurements of only the pitching and plunging variables, a multi-input/multi-output adaptive controller is designed to rapidly stabilize the pitching and plunging displacements). First, a bank of filters is designed to estimate the immeasurable state variables; the feedback gain matrix is appropriately tailored to ensure a commutativity property that is crucial to the control design and the stability analysis. Subsequently, the LECS and TECS deflection control inputs are designed in an adaptive backstepping framework via the help of a matrix decomposition scheme. This decomposition leads to an upper-triangular control gain matrix that is exploited to design singularity-free control laws that avoid algebraic loops. This control strategy can rapidly suppress the pitching and plunging nonlinear aeroelastic oscillations and its performance is comparable to existing techniques, while compensating for more uncertainty and using fewer measurements than existing schemes. The controller developed here is proven to be globally asymptotically stable via a Lyapunov-based analysis.

The rest of this paper is organized as follows. In Sec. II, the system dynamics are introduced. In Sec. III, we describe the control objective. In Sec. IV, the state-estimation strategy is designed. Section V deals with control design and stability analysis, along with signal-chasing. Section VI presents the simulation results, and we close in Sec. VII with conclusions.

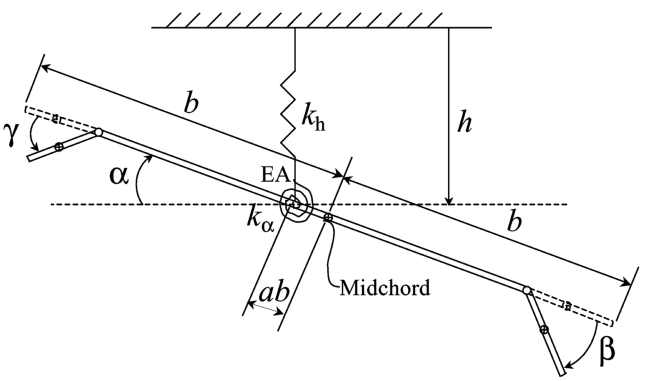

Fig. 1 Two-DOF aeroelastic system with both leading- and trailing-edge control surfaces.

II. Configuration of the 2-D Wing Aeroelastic Model

A schematic for a prototypical two-degree-of-freedom pitch-plunge wing section with LECS and TECS is presented in Fig. 1. The control inputs are the deflection of the leading- and trailing-edge flaps. The equations of motion for this system are given by [8,24,28]

$$\begin{bmatrix} m_T & m_w x_\alpha b \\ m_w x_\alpha b & I_\alpha \end{bmatrix}\begin{bmatrix} \ddot{h} \\ \ddot{\alpha} \end{bmatrix} + \begin{bmatrix} c_h & 0 \\ 0 & c_\alpha \end{bmatrix}\begin{bmatrix} \dot{h} \\ \dot{\alpha} \end{bmatrix} + \begin{bmatrix} k_h & 0 \\ 0 & k_\alpha(\alpha) \end{bmatrix}\begin{bmatrix} h \\ \alpha \end{bmatrix} = \begin{bmatrix} -L \\ M \end{bmatrix} \tag{1}$$

where $h(t)$ denotes the plunge displacement (positive downward); $\alpha(t)$ is the pitch angle (measured from the horizontal at the elastic axis of the airfoil, positive nose-up); $\beta(t)$ and $\gamma(t)$ are, respectively, the TECS and LECS deflections (measured from the axis created by the airfoil at the control flap hinge, positive flap-down), k_h and $k_\alpha(\alpha)$ are the linear and nonlinear stiffness of the plunging and pitching springs, respectively, attached to the elastic axis of the airfoil; and $k_\alpha(\alpha)$ denotes a continuous, linear parameterizable nonlinearity (i.e., the aeroelastic system has a continuous nonlinear restoring moment in the pitch degree of freedom). This polynomial stiffness term was derived by [29]. The model also considers structural damping, identified by the parameters c_h and c_α. The high-frequency dynamics of the control surfaces were neglected in this work, therefore, the aerodynamic forces and moments created by the control surface deflections are modeled as loads acting at the elastic axis [24]. In Eq. (1), the quasi-steady aerodynamic lift and moment, denoted by $L(\dot{h}, \dot{\alpha}, h, \alpha, \beta, \gamma)$ and $M(\dot{h}, \dot{\alpha}, h, \alpha, \beta, \gamma)$, respectively, are modeled as

$$\begin{aligned} L &= \rho U^2 bsC_{l\alpha}\left[\alpha + \frac{\dot{h}}{U} + \left(\frac{1}{2} - a\right)b\frac{\dot{\alpha}}{U}\right] + \rho U^2 bsC_{l\beta}\beta \\ &\quad + \rho U^2 bsC_{l\gamma}\gamma \\ M &= \rho U^2 b^2 sC_{m\alpha-\text{eff}}\left[\alpha + \frac{\dot{h}}{U} + \left(\frac{1}{2} - a\right)b\frac{\dot{\alpha}}{U}\right] \\ &\quad + \rho U^2 b^2 sC_{m\beta-\text{eff}}\beta + \rho U^2 b^2 sC_{m\gamma-\text{eff}}\gamma \end{aligned} \tag{2}$$

where $C_{m\alpha-\text{eff}}$, $C_{m\beta-\text{eff}}$, and $C_{m\gamma-\text{eff}}$ are the effective control moment derivatives [24] about the elastic axis, due to the angle of attack and trailing- and leading-edge control surface deflections, respectively, and are defined in the Appendix. The governing equations can be transformed using Eqs. (1) and (2) into the following form that is amenable to output feedback design:

$$\dot{\mathbf{x}} = \mathbf{A}\mathbf{x} + \bar{\mathbf{W}}(\mathbf{y}, \boldsymbol{\phi}) + \begin{bmatrix} 0_2 \\ \mathbf{G}_\mu \end{bmatrix}\mathbf{u} \qquad \mathbf{y} = \begin{bmatrix} \mathbf{I}_2 & \mathbf{0}_2 \end{bmatrix}\mathbf{x} = \mathbf{C}\mathbf{x} \tag{3}$$

where

$$\mathbf{x} \triangleq [\alpha(t) \quad h(t) \quad \dot{\alpha}(t) + c_4\alpha(t) + c_3 h(t) \quad \dot{h}(t) + c_2\alpha(t) + c_1 h(t)]^T \in \Re^4$$

is a vector of system states; $\mathbf{y}(\mathbf{t}) \triangleq [\alpha(t) \quad h(t)]^T \in \Re^2$ denotes the output vector;

$$\mathbf{u}(\mathbf{t}) = [u_1 \quad u_2] \triangleq U^2[\beta(t) \quad \gamma(t)] \in \Re^2$$

denotes the control input vector; $\bar{\mathbf{W}}(\mathbf{y}, \boldsymbol{\phi}) \in \Re^4$ is an auxiliary vector that captures the system nonlinearities; and $\mathbf{G}_\mu \in \Re^{2\times 2}$ is a constant nonsingular (but sign-indefinite), nonsymmetric, gain matrix. We

note here that the notations $\mathbf{0}_j$ and $\mathbf{I}_j$ denote, respectively, the zero and identity matrices of dimension j. The matrices $\mathbf{A}$ and $\mathbf{G}_\mu$ and the vector $\bar{\mathbf{W}}(\mathbf{y}, \boldsymbol{\phi})$ have the following structure:

$$\mathbf{A} = \begin{bmatrix} 0_2 & I_2 \\ 0_2 & 0_2 \end{bmatrix}, \qquad \bar{\mathbf{W}}(\mathbf{y}, \boldsymbol{\phi}) = \begin{bmatrix} -c_4\alpha - c_3 h \\ -c_2\alpha - c_1 h \\ -q(\alpha)\alpha - \kappa_4 U^2\alpha + \kappa_3 h \\ -p(\alpha)\alpha - \kappa_2 U^2\alpha + \kappa_1 h \end{bmatrix}$$
$$\mathbf{G}_\mu = \begin{bmatrix} g_{11} & g_{12} \\ g_{21} & g_{22} \end{bmatrix} \tag{4}$$

where the constant matrix entries g_{jk}, the constants κ_i, c_i $\forall\ i = 1, \ldots, 4$, and the linearly parameterizable functions $q(\alpha)$, $p(\alpha)$ due to the pitching stiffness nonlinearity are explicitly defined in the Appendix. In Eq. (3), $\bar{\mathbf{W}}(\mathbf{y}, \boldsymbol{\phi})$ can be linearly parameterized as follows:

$$\bar{\mathbf{W}}(\mathbf{y}, \boldsymbol{\phi}) = \mathbf{W}(\mathbf{y})\boldsymbol{\phi} = \sum_{j=1}^{p} \boldsymbol{\phi}_j \mathbf{W}_j(\mathbf{y})$$
$$= \sum_{j=1}^{p} \boldsymbol{\phi}_j \begin{bmatrix} W_{j,1}(y) & W_{j,2}(y) & W_{j,3}(y) & W_{j,4}(y) \end{bmatrix}^T \tag{5}$$

where $\boldsymbol{\phi} \in \Re^p$ is a vector of constant unknowns, with p being a positive integer; $\mathbf{W}(\mathbf{y}) \in \Re^{4\times p}$ is a measurable nonlinear regression matrix; the notation $\mathbf{W}_j(\cdot) \in \Re^p$ denotes the jth column of the regression matrix; and $W_{j,i}(y)$ denotes the ith element of $\mathbf{W}_j$. In Eq. (4), because both the leading principal minors g_{11} and $\Delta \triangleq \det(\mathbf{G}_\mu)$ of the matrix $\mathbf{G}_\mu$ are nonzero, we use a matrix decomposition introduced in [30] to obtain $\mathbf{G}_\mu = \mathbf{S}\mathbf{D}\bar{\mathbf{U}}$, where $\mathbf{S}$ is a symmetric positive-definite (PD) matrix, $\mathbf{D}$ is a diagonal matrix with its nonzero elements belonging to the set $\{+1, -1\}$, and $\bar{\mathbf{U}}$ is a unity upper-triangular matrix. From the solution of a nonlinear system of equations, $\mathbf{S}$, $\mathbf{D}$, and $\bar{\mathbf{U}}$ are obtained as follows:

$$\mathbf{S}(\boldsymbol{\theta}_2) = \begin{bmatrix} |g_{11}| & \operatorname{sign}(g_{11})g_{21} \\ \operatorname{sign}(g_{11})g_{21} & \operatorname{sign}(g_{11})\operatorname{sign}(\Delta)\{g_{22} - g_{11}^{-1}g_{21}[g_{12} - g_{21}\operatorname{sign}(\Delta)]\} \end{bmatrix} \qquad \mathbf{D}(\boldsymbol{\theta}_2) = \begin{bmatrix} \operatorname{sign}(g_{11}) & 0 \\ 0 & \operatorname{sign}(g_{11})\operatorname{sign}(\Delta) \end{bmatrix}$$
$$\bar{\mathbf{U}}(\boldsymbol{\theta}_2) = \begin{bmatrix} 1 & \frac{|g_{11}^{-1}|[g_{12} - g_{21}\operatorname{sign}(\Delta)]}{\operatorname{sign}(g_{11})} \\ 0 & 1 \end{bmatrix} \tag{6}$$

where the notation $\operatorname{sign}(\cdot)$ denotes the standard signum function. For purposes of control design, we will assume that the signs of the leading principal minors of the high-frequency gain matrix $\mathbf{G}_\mu$ are known, that is, the diagonal matrix $\mathbf{D}(\boldsymbol{\theta}_2)$ is assumed to be known.

III. Control Objective

Provided the structure of the aeroelastic model is known, the control objective is to design a control strategy to drive the pitch angle $\alpha(t)$ and plunge displacement $h(t)$ to zero, while adaptively compensating for uncertainties in all parameters of the model and the nonlinearity. We assume that the only measurements available are the pitching $\alpha(t)$ and plunging $h(t)$ displacements, and we compensate for the remaining states via the use of state estimators. First, we define a tracking error $\mathbf{e}(\mathbf{t}) \in \Re^2$ as follows:

$$\mathbf{e} = \mathbf{y} - \mathbf{y}_d \tag{7}$$

where $\mathbf{y}(t)$ denotes the output vector previously defined in Eq. (3), and $\mathbf{y}_d(t) \in \mathcal{C}^2$ denotes a sufficiently smooth, bounded-desired output vector. The smoothness requirement is motivated by the subsequent control design. To suppress aeroelastic vibrations, $\mathbf{y}_d(t)$ may be chosen to be identically zero over all time or one may want to define a desirable smooth trajectory along which $\mathbf{y}(t)$ may be driven to the origin. Next, we define a state-estimation error $\boldsymbol{\varepsilon}(\mathbf{t}) = [\boldsymbol{\varepsilon}_u \quad \boldsymbol{\varepsilon}_b]^T \in \Re^4$ as follows:

$$\boldsymbol{\varepsilon} = \mathbf{x} - \hat{\mathbf{x}} \tag{8}$$

where $\mathbf{x}(t)$ is the state vector previously defined in Eq. (3) and $\hat{\mathbf{x}}(\mathbf{t}) = [\hat{\mathbf{x}}_u \quad \hat{\mathbf{x}}_b]^T \in \Re^4$ is a state-estimation vector that is yet to be designed. Motivated by our desire to compensate for parameter uncertainty, we define parameter-estimation error signals $\tilde{\boldsymbol{\psi}}_1(t) \in \Re^{p_1}$ and $\tilde{\boldsymbol{\psi}}_2(t) \in \Re^{p_2}$ as follows:

$$\tilde{\boldsymbol{\psi}}_1 = \boldsymbol{\psi}_1 - \hat{\boldsymbol{\psi}}_1 \qquad \tilde{\boldsymbol{\psi}}_2 = \boldsymbol{\psi}_2 - \hat{\boldsymbol{\psi}}_2 \tag{9}$$

where $\boldsymbol{\psi}_1 \in \Re^{p_1}$ and $\boldsymbol{\psi}_2 \in \Re^{p_2}$ are unknown constant vectors and $\hat{\boldsymbol{\psi}}_1(t)$ and $\hat{\boldsymbol{\psi}}_2(t)$ are their corresponding estimates that will be subsequently generated dynamically. It is to be noted that p_1 and p_2 are nonnegative integers for which the values are determined through the structure and extent of uncertainty in the plant and the control scheme employed.

IV. State-Estimation Strategy

As shown in [20], the entire state of the system is observable from a measurement of the pitch-angle variable only. However, because we would like to rapidly stabilize the pitching and plunging displacements in an adaptive framework, we assume that both the pitching and plunging variables are available for measurement, which allows many possibilities for selection of estimator gain design. However, the problem of uncertainty in the parameters and our desire to construct an exponentially stable estimation error restricts us to the following structure for the gain matrix:

$$\mathbf{K}_o = [k_{o1}\mathbf{I}_2 \quad k_{o2}\mathbf{I}_2]^T \in \Re^{4\times 2}$$

where the scalars k_{o1} and k_{o2} are chosen such that $\mathbf{A}_0 = \mathbf{A} - \mathbf{K}_o\mathbf{C}$ is Hurwitz. Following the approach in [31], the filter

$$\boldsymbol{\zeta}_0 = [\zeta_{0,1} \quad \zeta_{0,2} \quad \zeta_{0,3} \quad \zeta_{0,4}]^T \in \Re^4$$

is designed for observing the unexcited linear system dynamics:

$$\dot{\boldsymbol{\zeta}}_0 = \mathbf{A}\boldsymbol{\zeta}_0 + \mathbf{K}_o\mathbf{C}(\mathbf{x} - \boldsymbol{\zeta}_0) \tag{10}$$

Because $\mathbf{A}$ is known and $\mathbf{C}\mathbf{x} = \mathbf{y}$ is measurable, the design of Eq. (10) is readily implementable. Moving on to the second term in the first equation of Eq. (3), one can exploit the linear parameterization of Eq. (5) and the fact that $\mathbf{A}_0$ is Hurwitz, to design a set of implementable filters

$$\boldsymbol{\zeta}_j(\mathbf{t}) = [\zeta_{j,1} \quad \zeta_{j,2} \quad \zeta_{j,3} \quad \zeta_{j,4}]^T \in \Re^4$$

as follows:

$$\dot{\boldsymbol{\zeta}}_j = \mathbf{A}_0\boldsymbol{\zeta}_j + \mathbf{W}_j(\mathbf{y}) \quad \forall\ j = 1 \ldots p \tag{11}$$

Finally, one can implement the following set of implementable filters $\boldsymbol{\upsilon} = [\,\boldsymbol{\upsilon}_u \quad \boldsymbol{\upsilon}_b\,]^T \in \Re^4$ as follows:

$$\dot{\boldsymbol{\upsilon}} = \begin{bmatrix} \dot{\boldsymbol{\upsilon}}_u \\ \dot{\boldsymbol{\upsilon}}_b \end{bmatrix} = \mathbf{A}_0\boldsymbol{\upsilon} + \begin{bmatrix} \mathbf{0}_2 \\ \mathbf{I}_2 \end{bmatrix}\mathbf{u} \tag{12}$$

We note here that it is straightforward to guarantee the boundedness of the filter variables $\boldsymbol{\zeta}_0(t)$, $\boldsymbol{\zeta}_j(t)$, and $\boldsymbol{\upsilon}(t)$, provided $\mathbf{y}(t)$ and $\mathbf{u}(t)$ remain bounded. Given Eqs. (10–12), an immeasurable state estimate $\hat{\mathbf{x}}(\mathbf{t})$ can be patched together as follows:

$$\hat{\mathbf{x}} = \boldsymbol{\zeta}_0 + \sum_{j=1}^{p} \boldsymbol{\phi}_j\boldsymbol{\zeta}_j + \begin{bmatrix} \mathbf{G}_\mu & \mathbf{0}_2 \\ \mathbf{0}_2 & \mathbf{G}_\mu \end{bmatrix}\boldsymbol{\upsilon} \tag{13}$$

After taking the time derivative of Eq. (13) along with the dynamics of Eqs. (10–12), we obtain the following expression:

$$\begin{aligned}\dot{\hat{\mathbf{x}}} &= \mathbf{A}\boldsymbol{\zeta}_0 + \mathbf{K}_o\mathbf{C}(\mathbf{x} - \boldsymbol{\zeta}_0) + \sum_{j=1}^{p} \boldsymbol{\phi}_j[\mathbf{A}_0\boldsymbol{\zeta}_j + \mathbf{W}_j(\mathbf{y})] \\ &\quad + \begin{bmatrix} \mathbf{G}_\mu & \mathbf{0}_2 \\ \mathbf{0}_2 & \mathbf{G}_\mu \end{bmatrix}\left(\mathbf{A}_0\boldsymbol{\upsilon} + \begin{bmatrix} \mathbf{0}_2 \\ \mathbf{I}_2 \end{bmatrix}\mathbf{u}\right)\end{aligned} \tag{14}$$

The special choice for the structure of the gain matrix $\mathbf{K}_o$ assures the following important commutation property:

$$\begin{bmatrix} \mathbf{G}_\mu & \mathbf{0}_2 \\ \mathbf{0}_2 & \mathbf{G}_\mu \end{bmatrix}\mathbf{A}_0 = \begin{bmatrix} \mathbf{G}_\mu & \mathbf{0}_2 \\ \mathbf{0}_2 & \mathbf{G}_\mu \end{bmatrix}\begin{bmatrix} -k_{o1}\mathbf{I}_2 & \mathbf{I}_2 \\ -k_{o2}\mathbf{I}_2 & \mathbf{0}_2 \end{bmatrix} = \mathbf{A}_0\begin{bmatrix} \mathbf{G}_\mu & \mathbf{0}_2 \\ \mathbf{0}_2 & \mathbf{G}_\mu \end{bmatrix} \tag{15}$$

By exploiting the aforementioned property, one can write the dynamics of Eq. (14) in the following convenient form:

$$\begin{aligned}\dot{\hat{x}} &= \mathbf{A}_0\left(\boldsymbol{\zeta}_0 + \sum_{j=1}^{p} \boldsymbol{\phi}_j\boldsymbol{\zeta}_j + \begin{bmatrix} \mathbf{G}_\mu & \mathbf{0}_2 \\ \mathbf{0}_2 & \mathbf{G}_\mu \end{bmatrix}\boldsymbol{\upsilon}\right) + \mathbf{K}_o\mathbf{C}\mathbf{x} \\ &\quad + \sum_{j=1}^{p} \boldsymbol{\phi}_j\mathbf{W}_j(\mathbf{y}) + \begin{bmatrix} \mathbf{0}_2 \\ \mathbf{G}_\mu \end{bmatrix}\mathbf{u} = \mathbf{A}_0\hat{\mathbf{x}} + \mathbf{K}_o\mathbf{C}\mathbf{x} \\ &\quad + \sum_{j=1}^{p} \boldsymbol{\phi}_j\mathbf{W}_j(\mathbf{y}) + \begin{bmatrix} \mathbf{0}_2 \\ \mathbf{G}_\mu \end{bmatrix}\mathbf{u}\end{aligned} \tag{16}$$

By taking the derivative of state-estimation error (8) and substituting for the dynamics of Eqs. (3) and (16), we obtain the following exponentially stable estimation error system:

$$\dot{\boldsymbol{\varepsilon}} = \mathbf{A}_0\boldsymbol{\varepsilon} \tag{17}$$

Although the state estimate is immeasurable, the importance of this scheme lies in the linear parameterizability of the right-hand side of the expression of Eq. (13) and in the exponential stability of the estimation error.

Remark 1: As an alternative way of designing the state-estimation strategy, one can implement the following set of implementable filters $\boldsymbol{\upsilon}_{ij} = [\,\boldsymbol{\upsilon}_{ij}^u \quad \boldsymbol{\upsilon}_{ij}^b\,]^T \in \Re^4\ \forall\ i = 1, 2$ and $j = 1, 2$ as follows:

$$\dot{\boldsymbol{\upsilon}}_{ij} = \mathbf{A}_0\boldsymbol{\upsilon}_{ij} + \mathbf{e}_{2+i}u_j \tag{18}$$

where $\mathbf{e}_i$ denotes the ith principal basis vector. The remaining filters are designed in the same way as in Eqs. (10) and (11). Here, $\mathbf{A}_0 = \mathbf{A} - \mathbf{K}_o\mathbf{C}$ is made Hurwitz by a proper choice of the gain matrix $\mathbf{K}_o$; because there is no restriction on the structure of $\mathbf{K}_o$, the eigenvalues of the state estimator can be arbitrarily placed. An immeasurable state estimate $\hat{\mathbf{x}}(\mathbf{t})$ can now be patched together as follows:

$$\hat{\mathbf{x}} = \boldsymbol{\zeta}_0 + \sum_{j=1}^{p} \boldsymbol{\phi}_j\boldsymbol{\zeta}_j + \sum_{i=1}^{2}\sum_{j=1}^{2} g_{ij}\boldsymbol{\upsilon}_{ij} \tag{19}$$

It can be readily verified that this leads to an exponentially stable estimation error system. However, this estimator is not implemented because it is not obvious how to design a bounded adaptive controller using such an estimator.

V. Adaptive Control Design and Stability Analysis

After differentiating the tracking error $\mathbf{e}(\mathbf{t})$ defined in Eq. (7) with respect to time along the open-loop dynamics given by Eq. (3), one obtains the following expression:

$$\begin{aligned}\dot{\mathbf{e}} &= \begin{bmatrix} \zeta_{0,3} \\ \zeta_{0,4} \end{bmatrix} + \sum_{j=1}^{p} \boldsymbol{\phi}_j\left(\begin{bmatrix} \boldsymbol{\zeta}_{j,3} \\ \boldsymbol{\zeta}_{j,4} \end{bmatrix} + \begin{bmatrix} \mathbf{W}_{j,1}(\mathbf{y}) \\ \mathbf{W}_{j,2}(\mathbf{y}) \end{bmatrix}\right) \\ &\quad + \mathbf{G}_\mu\boldsymbol{\upsilon}_b - \dot{\mathbf{y}}_d + \boldsymbol{\varepsilon}_b\end{aligned} \tag{20}$$

where we used the definitions of Eqs. (5), (8), and (13). After exploiting the matrix decomposition of Eq. (6) and adding and subtracting $k_1 e + d_1 e$ on the right-hand side of Eq. (20), one obtains the following succinct form for the open-loop error dynamics:

$$\mathbf{S}^{-1}\dot{\mathbf{e}} = -\mathbf{k}_1\mathbf{e} - d_1\mathbf{e} + \mathbf{S}^{-1}\boldsymbol{\varepsilon}_b + \mathbf{Y}_1\boldsymbol{\psi}_1 + \bar{\boldsymbol{\upsilon}}_b \tag{21}$$

where $\mathbf{k}_1 \in \Re^{2\times 2}$ is a control gain matrix, d_1 is a scalar positive control gain,

$$\bar{\boldsymbol{\upsilon}}_b = [\,\bar{\upsilon}_{b,1} \quad \bar{\upsilon}_{b,2}\,]^T \triangleq \mathbf{D}\boldsymbol{\upsilon}_b \in \Re^2$$

is an auxiliary measurable variable,

$$\mathbf{Y}_1(\mathbf{y}_d, \dot{\mathbf{y}}_d, \mathbf{y}, \boldsymbol{\zeta}_0, \boldsymbol{\zeta}_j, [\,\bar{\upsilon}_{b,2} \quad 0\,]^T) \in \Re^{2\times p_1}$$

is a measurable regression vector, $\boldsymbol{\psi}_1 \in \Re^{p_1}$ is an unknown parameter vector, and $\mathbf{Y}_1(\cdot)\boldsymbol{\psi}_1$ is explicitly defined as follows:

$$\begin{aligned}\mathbf{Y}_1\boldsymbol{\psi}_1 &= \mathbf{S}^{-1}\left[\begin{bmatrix} \zeta_{0,3} \\ \zeta_{0,4} \end{bmatrix} + \sum_{j=1}^{p} \boldsymbol{\phi}_j\left(\begin{bmatrix} \boldsymbol{\zeta}_{j,3} \\ \boldsymbol{\zeta}_{j,4} \end{bmatrix} + \begin{bmatrix} \mathbf{W}_{j,1}(\mathbf{y}) \\ \mathbf{W}_{j,2}(\mathbf{y}) \end{bmatrix}\right)\right] \\ &\quad + (\bar{\mathbf{U}} - \mathbf{I}_2)\bar{\boldsymbol{\upsilon}}_b - \mathbf{S}^{-1}\dot{\mathbf{y}}_d + \mathbf{k}_1\mathbf{e} + d_1\mathbf{e}\end{aligned} \tag{22}$$

We note here that $\bar{\mathbf{U}} - \mathbf{I}_2$ is a strictly upper-triangular matrix that leads to the second component of the regression vector $\mathbf{Y}_1(\cdot)$ being independent of $\bar{\upsilon}_{b,2}$. Motivated by the desire to use the backstepping technique, we define an error variable

$$\tilde{\boldsymbol{\upsilon}}_b \triangleq [\,\tilde{\upsilon}_{b,1} \quad \tilde{\upsilon}_{b,2}\,]^T = \bar{\boldsymbol{\upsilon}}_b - \bar{\boldsymbol{\upsilon}}_{bd} \tag{23}$$

where $\bar{\boldsymbol{\upsilon}}_{bd} = [\,\bar{\upsilon}_{bd,1} \quad \bar{\upsilon}_{bd,2}\,]^T \in \Re^2$ is a virtual control input that is designed as follows:

$$\bar{\boldsymbol{\upsilon}}_{bd} = -\mathbf{Y}_1[\mathbf{y}_d, \dot{\mathbf{y}}_d, \mathbf{y}, \boldsymbol{\zeta}_0, \boldsymbol{\zeta}_j, (\mathbf{U} - \mathbf{I}_2)\bar{\boldsymbol{\upsilon}}_b]\hat{\boldsymbol{\psi}}_1 \tag{24}$$

where $\hat{\boldsymbol{\psi}}_1(t)$ is dynamically generated as follows:

$$\dot{\hat{\boldsymbol{\psi}}}_1 = \Gamma_1\mathbf{Y}_1^T\mathbf{e} \tag{25}$$

where $\Gamma_1 \in \Re^{p_1\times p_1}$ is a positive-definite gain matrix. By adding and subtracting $\bar{\boldsymbol{\upsilon}}_{bd}(t)$ on the right-hand side of Eq. (21) and using Eq. (24), we can obtain

$$\mathbf{S}^{-1}\dot{\mathbf{e}} = -\mathbf{k}_1\mathbf{e} - d_1\mathbf{e} + \mathbf{S}^{-1}\boldsymbol{\varepsilon}_b + \mathbf{Y}_1\tilde{\boldsymbol{\psi}}_1 + \tilde{\boldsymbol{\upsilon}}_b \tag{26}$$

To analyze stability, we define an intermediate Lyapunov function $V(t)$ as follows:

$$V = \tfrac{1}{2}\mathbf{e}^T\mathbf{S}^{-1}\mathbf{e} + \tfrac{1}{2}\tilde{\boldsymbol{\psi}}_1^T\Gamma_1^{-1}\tilde{\boldsymbol{\psi}}_1 + \boldsymbol{\varepsilon}^T\mathbf{P}\boldsymbol{\varepsilon} \tag{27}$$

where $\mathbf{P} = \mathbf{P}^T$ is a PD matrix. The exponential stability of the ε dynamics guarantees the existence of such a matrix, because it is

known that given a PD symmetric matrix

$$\mathbf{Q} \triangleq \begin{bmatrix} \mathbf{I}_2 & \mathbf{0}_2 \\ \mathbf{0}_2 & \mathbf{I}_2 + d_1^{-1}(\mathbf{S}^{-1})^T\mathbf{S}^{-1} + d_2^{-1}\mathbf{I}_2 \end{bmatrix}$$

with d_1 and $\mathbf{S}$ as previously defined and $d_2 > 0$, one can find a PD symmetric matrix $\mathbf{P}$ such that

$$\mathbf{P}\mathbf{A}_0 + \mathbf{A}_0^T\mathbf{P} = -\mathbf{Q} \tag{28}$$

After taking the time derivative of $V(t)$ along the trajectories of Eqs. (25) and (26), one can obtain

$$\dot{V} = -\mathbf{e}^T\mathbf{k}_1\mathbf{e} + [\mathbf{e}^T\mathbf{S}^{-1}\boldsymbol{\varepsilon}_b - d_1\|\mathbf{e}\|^2] + \mathbf{e}^T\tilde{\boldsymbol{\upsilon}}_b - \boldsymbol{\varepsilon}^T\mathbf{Q}\boldsymbol{\varepsilon}$$

By using the preceding definition of $\mathbf{Q}$ and completing the squares on the bracketed term in the preceding equation, one can upperbound $\dot{V}(t)$ as follows:

$$\dot{V} \leq -k_{1,\min}\|\mathbf{e}\|^2 - \boldsymbol{\varepsilon}^T\mathbf{Q}_1\boldsymbol{\varepsilon} + \mathbf{e}^T\tilde{\boldsymbol{\upsilon}}_b \tag{29}$$

where

$$\mathbf{Q}_1 \triangleq \begin{bmatrix} \mathbf{I}_2 & \mathbf{0}_2 \\ \mathbf{0}_2 & \mathbf{I}_2 + d_2^{-1}\mathbf{I}_2 \end{bmatrix}$$

and $k_{1,\min}$ denotes the minimum eigenvalue of the gain matrix $\mathbf{k}_1$. Before one can proceed with the remainder of the design, we note here that the time derivative of the virtual control input $\bar{\upsilon}_{bd}(t)$ can be obtained as

$$\dot{\bar{\boldsymbol{\upsilon}}}_{bd} = \bar{\mathbf{Y}}_2(\cdot)\bar{\boldsymbol{\psi}}_2 + \frac{\partial\bar{\boldsymbol{\upsilon}}_{bd}}{\partial\mathbf{y}}\varepsilon_b \tag{30}$$

where

$$\bar{\mathbf{Y}}_2(\mathbf{y}, \dot{\mathbf{y}}_d, \ddot{\mathbf{y}}_d, \zeta_{0,3}, \zeta_{0,4}, \boldsymbol{\zeta}_{j,3}, \boldsymbol{\zeta}_{j,4}, \boldsymbol{\upsilon}, [u_2 \quad 0]^T) \in \Re^{2\times\bar{p}_2}$$

is a measurable regression vector, $\bar{\boldsymbol{\psi}}_2 \in \Re^{\bar{p}_2}$ is an unknown parameter vector, and $\bar{\mathbf{Y}}_2(\cdot)\bar{\boldsymbol{\psi}}_2$ is explicitly defined as follows:

$$\begin{aligned}\bar{\mathbf{Y}}_2\bar{\boldsymbol{\psi}}_2 &= \frac{\partial\bar{\boldsymbol{\upsilon}}_{bd}}{\partial\mathbf{y}_d}\dot{\mathbf{y}}_d + \frac{\partial\bar{\boldsymbol{\upsilon}}_{bd}}{\partial\dot{\mathbf{y}}_d}\ddot{\mathbf{y}}_d + \frac{\partial\bar{\boldsymbol{\upsilon}}_{bd}}{\partial\boldsymbol{\zeta}_0}\dot{\boldsymbol{\zeta}}_0 + \sum_{j=1}^{p}\frac{\partial\bar{\boldsymbol{\upsilon}}_{bd}}{\partial\boldsymbol{\zeta}_j}\dot{\boldsymbol{\zeta}}_j \\ &+ \frac{\partial\bar{\boldsymbol{\upsilon}}_{bd}}{\partial\hat{\boldsymbol{\psi}}_1}\Gamma_1\mathbf{Y}_1^T\mathbf{e} + \frac{\partial\bar{\boldsymbol{\upsilon}}_{bd}}{\partial\mathbf{y}}\left(\begin{bmatrix}\zeta_{0,3}\\ \zeta_{0,4}\end{bmatrix} + \sum_{j=1}^{p}\boldsymbol{\phi}_j\begin{bmatrix}\boldsymbol{\zeta}_{j,3}\\ \boldsymbol{\zeta}_{j,4}\end{bmatrix}\right. \\ &\left. + \mathbf{G}_\mu\boldsymbol{\upsilon}_b + \sum_{j=1}^{p}\boldsymbol{\phi}_j\begin{bmatrix}\mathbf{W}_{j,1}(\mathbf{y})\\ \mathbf{W}_{j,2}(\mathbf{y})\end{bmatrix}\right) + \frac{\partial\bar{\boldsymbol{\upsilon}}_{bd}}{\partial\bar{\boldsymbol{\upsilon}}_b}\dot{\bar{\boldsymbol{\upsilon}}}_b\end{aligned} \tag{31}$$

We note here that the last term in the preceding equation introduces the $u_2(t)$ dependence of $\bar{\mathbf{Y}}_2(\cdot)$, but only in the first row, because of the previously explained asymmetric structure of $Y_1(\cdot)$. We also remark here that the first term in Eq. (30) is linear in the unknown parameters and can be adaptively compensated, and the second term contains the immeasurable estimation error signal $\varepsilon_2(t)$ and must be nonlinearly damped out. To continue with the backstepping design, we take the time derivative of Eq. (23) along with the dynamics of Eq. (30) and the bottom two rows of Eq. (12) to obtain

$$\dot{\bar{\boldsymbol{\upsilon}}}_b = -k_{o2}\mathbf{D}\boldsymbol{\upsilon}_u + \mathbf{D}\mathbf{u} - \bar{\mathbf{Y}}_2(\cdot)\bar{\boldsymbol{\psi}}_2 - \frac{\partial\bar{\boldsymbol{\upsilon}}_{bd}}{\partial\mathbf{y}}\boldsymbol{\varepsilon}_b \tag{32}$$

where we have used the previously defined $\bar{\boldsymbol{\upsilon}}_b = \mathbf{D}\boldsymbol{\upsilon}_b$. After adding and subtracting appropriate feedback and damping terms on the right-hand side of Eq. (32), one obtains the following expression:

$$\begin{aligned}\dot{\bar{\boldsymbol{\upsilon}}}_b &= -\mathbf{k}_2\tilde{\boldsymbol{\upsilon}}_b + \mathbf{Y}_2\boldsymbol{\psi}_2 + \left[-\frac{\partial\bar{\boldsymbol{\upsilon}}_{bd}}{\partial\mathbf{y}}\boldsymbol{\varepsilon}_b - d_2\left(\frac{\partial\bar{\boldsymbol{\upsilon}}_{bd}}{\partial\mathbf{y}}\right)^T\left(\frac{\partial\bar{\boldsymbol{\upsilon}}_{bd}}{\partial\mathbf{y}}\right)\tilde{\boldsymbol{\upsilon}}_b\right] \\ &- \mathbf{e} + \mathbf{D}\mathbf{u}\end{aligned} \tag{33}$$

where $\mathbf{k}_2 \in \Re^{2\times2}$ is a positive-definite control gain matrix, d_2 is a scalar positive control gain,

$$\mathbf{Y}_2(\mathbf{y}, \dot{\mathbf{y}}_d, \ddot{\mathbf{y}}_d, \zeta_{0,3}, \zeta_{0,4}, \boldsymbol{\zeta}_{j,3}, \boldsymbol{\zeta}_{j,4}, \boldsymbol{\upsilon}, \tilde{\boldsymbol{\upsilon}}_b, [u_2 \quad 0]^T) \in \Re^{2\times p_2}$$

is a measurable regression vector, $\boldsymbol{\psi}_2 \in \Re^{p_2}$ is an unknown parameter vector, and $\mathbf{Y}_2(\cdot)\boldsymbol{\psi}_2$ is explicitly defined as follows:

$$\begin{aligned}\mathbf{Y}_2\boldsymbol{\psi}_2 &= \mathbf{k}_2\tilde{\boldsymbol{\upsilon}}_b - \bar{\mathbf{Y}}_2(\cdot)\bar{\boldsymbol{\psi}}_2 - k_{o2}\mathbf{D}\boldsymbol{\upsilon}_u \\ &+ d_2\left(\frac{\partial\bar{\boldsymbol{\upsilon}}_{bd}}{\partial\mathbf{y}}\right)^T\left(\frac{\partial\bar{\boldsymbol{\upsilon}}_{bd}}{\partial\mathbf{y}}\right)\tilde{\boldsymbol{\upsilon}}_b + \mathbf{e}\end{aligned} \tag{34}$$

Based on the structure of the dynamics of Eq. (33), the control input signal $\mathbf{u}(t)$ can be designed as

$$\mathbf{u} = -\mathbf{D}\mathbf{Y}_2\hat{\boldsymbol{\psi}}_2 \tag{35}$$

where the unknown parameters in $\hat{\boldsymbol{\psi}}_2(t)$ are dynamically estimated as follows:

$$\dot{\hat{\boldsymbol{\psi}}}_2 = \Gamma_2\mathbf{Y}_2^T\tilde{\boldsymbol{\upsilon}}_b \tag{36}$$

where $\Gamma_2 \in \Re^{p_2\times p_2}$ is a positive-definite gain matrix. After substituting the control input of Eq. (35) into Eq. (34), the closed-loop dynamics can be obtained as

$$\begin{aligned}\dot{\tilde{\boldsymbol{\upsilon}}}_b &= -\mathbf{k}_2\tilde{\boldsymbol{\upsilon}}_b + \mathbf{Y}_2\tilde{\boldsymbol{\psi}}_2 \\ &+ \left[-\frac{\partial\bar{\boldsymbol{\upsilon}}_{bd}}{\partial\mathbf{y}}\boldsymbol{\varepsilon}_b - d_2\left(\frac{\partial\bar{\boldsymbol{\upsilon}}_{bd}}{\partial\mathbf{y}}\right)^T\left(\frac{\partial\bar{\boldsymbol{\upsilon}}_{bd}}{\partial\mathbf{y}}\right)\tilde{\boldsymbol{\upsilon}}_b\right] - \mathbf{e}\end{aligned} \tag{37}$$

where we have exploited the fact that $\mathbf{D}^2 = \mathbf{I}_2$. In the preceding expression, the first term is a negative feedback term, the second term is the adaptive mismatch term, the last term is an interconnection buster between the dynamics of Eqs. (26) and (37), and the terms between brackets are a nonlinear damping pair [32] that will be used subsequently. Toward a final stability analysis, the function of Eq. (27) can be augmented as follows:

$$V_1 = V + \tfrac{1}{2}\tilde{\boldsymbol{\upsilon}}_b^T\tilde{\boldsymbol{\upsilon}}_b + \tfrac{1}{2}\tilde{\boldsymbol{\psi}}_2^T\Gamma_2^{-1}\tilde{\boldsymbol{\psi}}_2 \tag{38}$$

The time derivative of $V_1(t)$ along the closed-loop trajectories of Eqs. (36) and (37) yields the following upper bound:

$$\dot{V}_1 \leq -k_{1,\min}\|\mathbf{e}\|^2 - k_{2,\min}\|\tilde{\boldsymbol{\upsilon}}_b\|^2 - \|\boldsymbol{\varepsilon}\|^2 \tag{39}$$

where $k_{2,\min}$ denotes the minimum eigenvalue of the gain matrix $\mathbf{k}_2$ and we used the upper bound of Eq. (29) and the nonlinear damping argument. We now proceed carefully with boundedness and signal-chasing arguments. Because $\dot{V}_1(t)$ is negative semidefinite and $V_1(t)$ is positive definite, we can conclude that $V_1(t) \in \mathcal{L}_\infty$. Therefore, from the Lyapunov functions $V(t)$ and $V_1(t)$, it is easy to see that $\tilde{\boldsymbol{\psi}}_1(\mathbf{t})$, $\tilde{\boldsymbol{\psi}}_2(\mathbf{t}) \in \mathcal{L}_\infty$, $\mathbf{e}(\mathbf{t})$, $\tilde{\boldsymbol{\upsilon}}_b(\mathbf{t})$, and $\boldsymbol{\varepsilon}(\mathbf{t}) \in \mathcal{L}_\infty \cap \mathcal{L}_2$. From the apriori boundedness of $\mathbf{y}_d(t)$, $\boldsymbol{\psi}_1$, and $\boldsymbol{\psi}_2$, we can say that $\mathbf{y}(t)$, $\hat{\boldsymbol{\psi}}_1(t)$, and $\hat{\boldsymbol{\psi}}_2(t) \in \mathcal{L}_\infty$. From the structure of Eqs. (10) and (11) and the boundedness of $\mathbf{y}(t)$, one can easily see that $\boldsymbol{\zeta}_i(t) \in \mathcal{L}_\infty$ $\forall\ i = 0, \ldots, p$. Based on the output equation of Eq. (3), the definition of Eq. (8), and the fact that $\mathbf{y}(\mathbf{t})$ and $\boldsymbol{\varepsilon}(\mathbf{t}) \in \mathcal{L}_\infty$, it is clear that $\hat{\mathbf{x}}_u(\mathbf{t}) \in \mathcal{L}_\infty$. Then, from the definition of Eq. (13) and the preceding facts, one can see that $\boldsymbol{\upsilon}_u(\mathbf{t}) \in \mathcal{L}_\infty$. From Eq. (22), one can see that the second row of $\mathbf{Y}_1(\cdot)$ is only dependent upon signals for which the boundedness is guaranteed and therefore $\mathbf{Y}_{1,2}(\cdot) \in \mathcal{L}_\infty$. From Eq. (24), one can now claim that $\bar{\upsilon}_{bd,2}(t)$ is bounded. From the error definition of Eq. (23) and the fact that $\tilde{\boldsymbol{\upsilon}}_b(\mathbf{t}) \in \mathcal{L}_\infty$, it now implies that $\bar{\upsilon}_{b,2}(t)$ is bounded. Given the preceding facts and from Eq. (24), $\bar{\upsilon}_{bd,1}(t)$ is bounded. Again, the definition of Eq. (23) and previous boundedness assertions can be used to prove that $\bar{\upsilon}_{b,1}(t) \in \mathcal{L}_\infty$. Because the control input $u_2(t)$ is designed to be independent of $u_1(t)$ and only dependent on all previously bounded signals, we can say that $u_2(t) \in \mathcal{L}_\infty$. This boundedness of $u_2(t)$ coupled with all previous boundedness assertions can be used to state that $u_1(t)$ is bounded. From Eqs. (17), (26), and (37), one can state

that $\dot{\boldsymbol{\varepsilon}}(t)$, $\dot{\mathbf{e}}(t)$, and $\dot{\tilde{\boldsymbol{\upsilon}}}_b(t)$ are bounded, thus, $\boldsymbol{\varepsilon}(t)$, $\mathbf{e}(t)$, and $\tilde{\boldsymbol{\upsilon}}_b(t)$ are uniformly continuous. Thus, one can apply Barbalat's Lemma [33] to state that $\lim_{t\to\infty}\mathbf{e}(t)$, $\tilde{\boldsymbol{\upsilon}}_b(t)$, and $\boldsymbol{\varepsilon}(t) = 0$. Thus, the system is globally asymptotically stable and all signals in the plant, estimator, and controller stay bounded in closed-loop operation.

Remark 2: In a manner similar to that demonstrated in [23], the backstepping procedure allows for inclusion of actuator dynamics to the overall plant dynamics. When the actuator dynamics are faster (as is generally the case) than the remainder of the plant, it was observed that the evolution of the output is affected only minimally by inclusion of actuator dynamics in the overall design procedure.

VI. Simulations, Results, and Discussions

The nonlinear wing-section model was simulated using the dynamics of Eqs. (1) and (2), and the controller was implemented via Eqs. (24), (25), (35), and (36). To simulate a practical system, both the leading-edge $\gamma(t)$ and trailing-edge $\beta(t)$ flaps were saturated to vary between ± 15 deg. Similar to [24], the nonlinear pitch stiffness $k_\alpha(\alpha)$ was chosen to be represented by a second-order polynomial as follows:

$$k_\alpha(\alpha) = 12.77 + 53.47\alpha + 1003\alpha^2$$

The model parameters used are listed as follows [24]:

$$\rho = 1.225\ \text{kg}\cdot\text{m}^3 \qquad a = -0.6719 \qquad k_h = 2844\ \text{N}\cdot\text{m}^{-1}$$
$$s = 0.5945\ \text{m} \qquad m_T = 15.57\ \text{kg} \qquad b = 0.1905\ \text{m}$$
$$c_h = 27.43\ \text{N}\cdot\text{m}^{-1}\cdot\text{s}^{-1} \qquad c_\alpha = 0.0360\ \text{N}\cdot\text{s}$$
$$I_{cgw} = 0.04342\ \text{kg}\cdot\text{m}^2 \qquad m_w = 5.23\ \text{kg}$$
$$I_{cam} = 0.04697\ \text{kg}\cdot\text{m}^2 \qquad C_{l\gamma} = -0.1566 \qquad C_{l\alpha} = 6.757$$
$$C_{l\beta} = 3.774 \qquad C_{m\alpha} = 0 \qquad C_{m\beta} = -0.6719$$
$$I_\alpha = I_{cam} + I_{cgw} + m_w r_{cg}^2 \qquad C_{m\gamma} = -0.1005$$
$$r_{cg} = -b(.0998 + a)\ \text{m} \qquad x_a = r_{cg}/b$$

The initial conditions for pitch angle $\alpha(t)$ and plunge displacement $h(t)$ were chosen as

$$\alpha(0) = 5.729\ \text{deg} \qquad h(0) = 0\ \text{m}$$

and all other initial conditions were set to zero. The system was seen to have a flutter velocity of $U_F = 11.4\ \text{m}\cdot\text{s}^{-1}$. Two sets of simulations were run: the first at the subcritical flight speed of $U = 8\ \text{m}\cdot\text{s}^{-1}$ and the second set in postflutter condition, $U = 13.15\ \text{m}\cdot\text{s}^{-1}$. For both runs of the simulation, the observer gains are chosen to be $k_{o1} = 3.05e3$ and $k_{02} = 2.325e5$, such that the observer poles are located at $p_{o1} = p_{o2} = -2.97e3$ and $p_{o3} = p_{o4} = -7.8e1$. As is generally the case, the controller and parameter estimator gains are different for each regime.

The first simulation is run at preflutter velocity (i.e., $U = 8\ \text{m}\cdot\text{s}^{-1}$). The control gains, damping coefficients, and settling-time constants were chosen as follows:

$$\Gamma_1 = 20\mathbf{I}_{63} \qquad \mathbf{k}_1 = \text{diag}\{9, 25\} \qquad d_1 = 1e-3$$
$$\Gamma_2 = 40\mathbf{I}_{48} \qquad \mathbf{k}_2 = \text{diag}\{3, 25\} \qquad d_2 = 1e-3$$

Figure 2 shows the open-loop response of the system, which has a settling time of approximately 8 s for both pitch and plunge displacements. Figure 3 shows the pitch and plunge displacements and trailing-edge actuator response of the system with single actuator control (i.e., trailing-edge flap actuated at $t = 0$ s). It can be noticed that the pitch angle settles within 1 s, and the plunge displacement settles in around 1.2 s. Figure 4 shows the responses when both the LECS and TECS are actuated at $t = 0$ s. It can be seen that both the pitch angle and plunge displacement have settling times less than 0.75 s.

The second simulation is run at postflutter velocity (i.e., $U = 13.15\ \text{ms}^{-1}$) with similar initial conditions. To obtain the LCO,

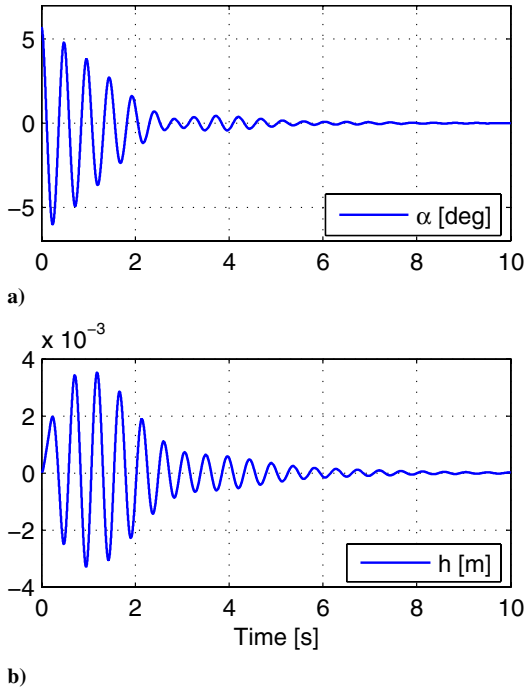

Fig. 2 Time evolution of open-loop pitching and plunging deflections for $U = 8\ \text{m}\cdot\text{s}^{-1} < U_F = 11.4\ \text{m}\cdot\text{s}^{-1}$.

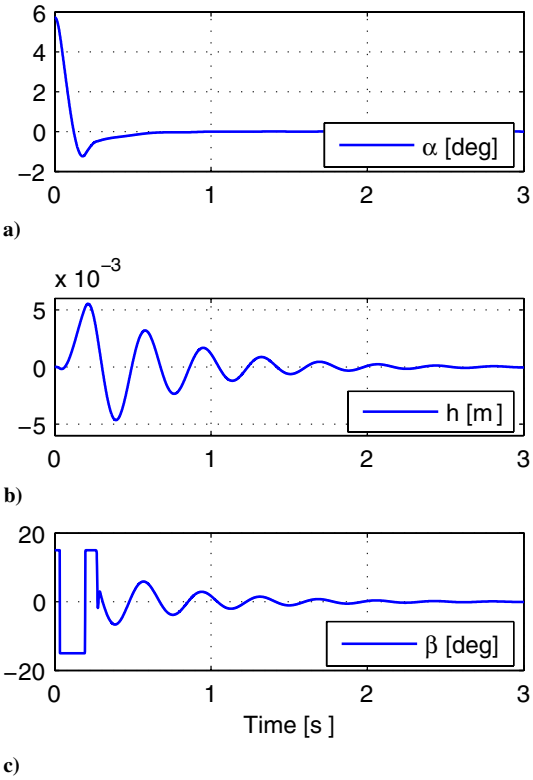

Fig. 3 Closed-loop pitching, plunging, and control surface deflection with trailing-edge flap actuation for $U = 8\ \text{m}\cdot\text{s}^{-1} < U_F$.

the system is kept in open loop for 15 s and then the loop is closed. The control gains, damping coefficients, and settling-time constants were chosen as follows:

$$\Gamma_1 = \mathbf{I}_{63} \qquad \mathbf{k}_1 = \text{diag}\{19, 25e2\} \qquad d_1 = 1e-3$$
$$\Gamma_2 = 0.4\mathbf{I}_{48} \qquad \mathbf{k}_2 = \text{diag}\{1, 25\} \qquad d_2 = 1e-3$$

At $t = 15$ s, the trailing-edge flap is switched on and the pitching

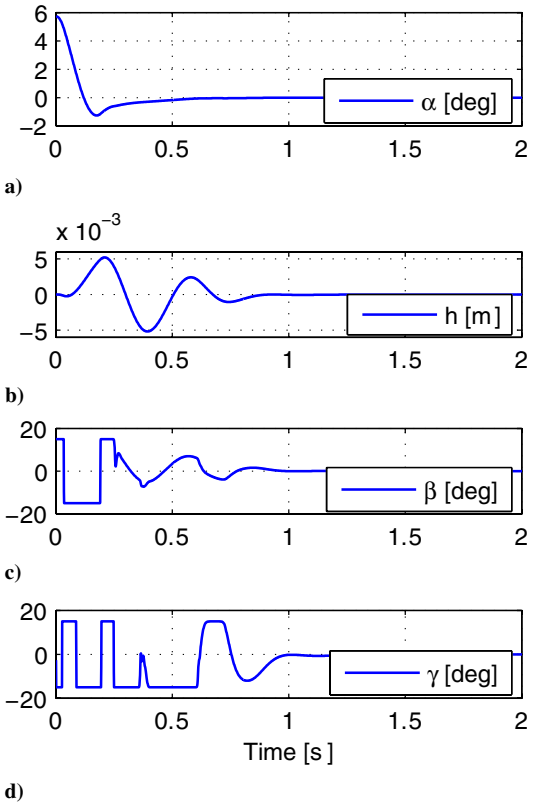

Fig. 4 Closed-loop pitching, plunging, and control surface deflections with both trailing- and leading-edge flap actuations for $U = 8\ \text{m} \cdot \text{s}^{-1} < U_F = 11.4\ \text{m} \cdot \text{s}^{-1}$.

LCO is suppressed before plunging LCO, whereas the plunging LCO takes around 3 s to settle, which can be observed in Fig. 5. Better results can be observed when both the trailing- and leading-edge actuators are switched on at $t = 15$ s, which is shown in Fig. 6. The pitching and plunging LCOs are suppressed in approximately 2 s.

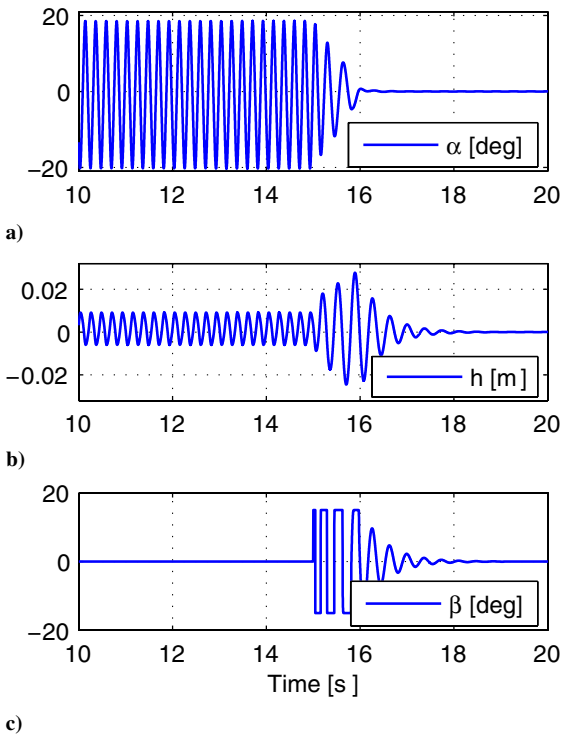

Fig. 5 Closed-loop pitching, plunging, and control surface deflections with only trailing-edge flap actuated at $t = 15$ s for $U = 13.28\ \text{m} \cdot \text{s}^{-1} < U_F = 11.4\ \text{m} \cdot \text{s}^{-1}$.

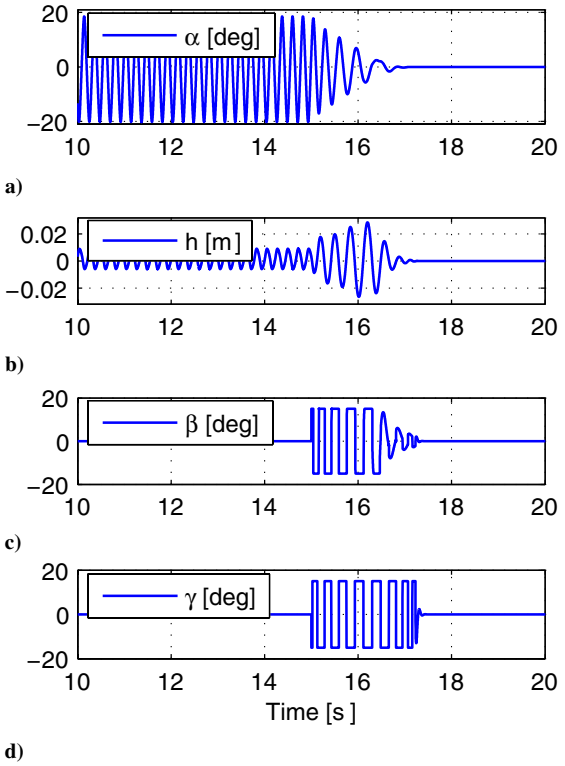

Fig. 6 Closed-loop pitching, plunging, and control surface deflections with both trailing-edge and leading-edge flaps actuated at $t = 15$ s for $U = 13.28\ \text{m} \cdot \text{s}^{-1} < U_F = 11.4\ \text{m} \cdot \text{s}^{-1}$.

VII. Conclusions

Results related to the adaptive output feedback control of a nonlinear plunging-pitching wing-section operation in an incompressible flight speed were presented here. In this paper, a multivariable control strategy is implemented via leading-edge γ and trailing-edge β control surfaces. The performance of the adaptive control is analyzed and simulations show that the control strategy effectively controls the pitching and plunging even after the system is allowed to evolve into limit-cycle oscillations. Even with compensating for uncertainty and only measuring the output variables, the performance of the controller compares favorably with results obtained in [24,25]. As pointed out in [24], their approach is not very effective when the freestream velocity approaches 17 m/s. A similar degradation in performance was observed for our scheme when approaching that freestream velocity. However, this is to be expected, because we are using similar control actuation as used in [24] but with more restricted measurements (pitching and plunging velocities are not measurable) and with more parameters being allowed to be uncertain.

The adaptive output feedback control algorithm for the elastic wing with leading- and trailing-edge flaps can be considered as a generalization of [23,25]. Therefore, it would be desirable to show that the designed controller can be applied (with some modification) to the two previous cases and formulate recommendations summarizing this modification. A modification may be straightforward for the design of [23] because the SDU decomposition used in this paper simplifies to writing the scalar high-frequency gain in the single-input/single-output case as the product of its sign and its magnitude. However, we believe that it may not be straightforward to generalize this design to the adaptive full-state feedback design of [25]. Because the control design in [25] is not based upon a backstepping procedure and owing to the fact that the backstepping-based output feedback controller proposed here requires significant overparameterization, it is not clear to us how to proceed with simplifying that for the full-state case. Future work will concentrate on addressing this issue, among others. Other issues would be to determine adaptive strategies in which there is more freedom in

placing state-estimator poles. We would also concern ourselves with strategies that rely only on either the pitching or the plunging variable and not both simultaneously.

Although a choice of the backstepping technique may be advantageous for many designs, there are also restrictions that need to be known and considered. Advantages of a backstepping method allow the designer to easily consider nonlinearities and incorporate adaptive design when the nonlinearities are affine in the parameters. In addition, the procedure relies on a Lyapunov-based method and it allows facile design of controllers that lead to global stability results; whenever that is not possible, the Lyapunov procedure allows for computation of an explicit region of attraction. Another big advantage is that the procedure is systematic and is amenable to automation. In addition, the backstepping technique allows for facile extension of the system to include additional dynamics introduced by actuators or some class of periodic disturbances. However, restrictions include linear dependence of the model on unknown parameters for adaptive design, as well as the restriction of output feedback design to systems with nonlinearities depending only on output variables. Other disadvantages include significant over-parameterization, which not only leads to increase of the system order (which may be a problem if a slow microprocessor is used in a digital implementation), but it also leads to a problem of assigning systematic ways to assign controller parameters to achieve desired system characteristics in the closed loop.

Appendix: Definitions for Model Constants

The constants κ_i, $c_i\ \forall\ i = 1, 2, 3, 4$, $g_{jk}\ \forall\ j\ k = 1, 2$, $p(\alpha)$, and $q(\alpha)$ are defined as

$$g_{11} = D^{-1}[m_w x_\alpha b^2 \rho s C_{l\beta} + m_T \rho s b^2 C_{m\beta-\text{eff}}]$$

$$g_{12} = D^{-1}[m_w x_\alpha b^2 \rho s C_{l\gamma} + m_T \rho s b^2 C_{m\gamma-\text{eff}}]$$

$$g_{21} = D^{-1}[-I_\alpha \rho b s C_{l\beta} - m_w x_\alpha b^3 s \rho C_{m\beta-\text{eff}}]$$

$$g_{22} = D^{-1}[-I_\alpha \rho b s C_{l\gamma} - m_w x_\alpha b^3 s \rho C_{m\gamma-\text{eff}}]$$

$$D = m_T I_\alpha - m_w^2 x_\alpha^2 b^2 \qquad \kappa_1 = I_\alpha k_h D^{-1}$$

$$\kappa_2 = D^{-1}(I_\alpha \rho b s C_{l\alpha} + m_w x_\alpha \rho s b^3 C_{m\alpha-\text{eff}})$$

$$\kappa_3 = -D^{-1} m_w x_\alpha b k_h$$

$$\kappa_4 = -D^{-1}(m_w x_\alpha \rho b^2 s C_{l\alpha} + m_T \rho s b^2 C_{m\alpha-\text{eff}})$$

$$p(\alpha) = -m_w x_\alpha b k_\alpha(\alpha) D^{-1} \qquad q(\alpha) = m_T k_\alpha(\alpha) D^{-1}$$

$$k_\alpha(\alpha) = A + B\alpha + C\alpha^2$$

$$c_1 = D^{-1}[I_\alpha(c_h + \rho U b s C_{l\alpha}) + m_w x_\alpha \rho U s b^3 C_{m\alpha-\text{eff}}]$$

$$c_2 = D^{-1}[I_\alpha \rho U b^2 s C_{l\alpha}(0.5 - a) - m_w x_\alpha b c_\alpha + m_w x_\alpha \rho U s b^4 C_{m\alpha-\text{eff}}(0.5 - a)]$$

$$c_3 = D^{-1}[-m_w x_\alpha b(c_h + \rho U b s C_{l\alpha}) - m_T \rho U s b^2 C_{m\alpha-\text{eff}}]$$

$$c_4 = D^{-1}\{m_T[c_\alpha - \rho U s b^3 C_{m\alpha-\text{eff}}(0.5 - a)] - m_w x_\alpha \rho U s b^3 C_{l\alpha}(0.5 - a)\}$$

$$C_{m\alpha-\text{eff}} = \left(\tfrac{1}{2} + a\right) C_{l\alpha} + 2C_{m\alpha}$$

$$C_{m\beta-\text{eff}} = \left(\tfrac{1}{2} + a\right) C_{l\beta} + 2C_{m\beta}$$

$$C_{m\gamma-\text{eff}} = \left(\tfrac{1}{2} + a\right) C_{l\gamma} + 2C_{m\gamma}$$

Explicit expressions for $W(\cdot)$, ϕ, $Y_1(\cdot)$, ψ_1, $Y_2(\cdot)$, and ψ_2 are available from the authors.

References

[1] Librescu, L., and Marzocca, P., "Advances in the Linear/Nonlinear Control of Aeroelastic Structural Systems," *Acta Mechanica*, Vol. 178, Nos. 3-4, 2005, pp. 147–186.

[2] Noll, T. E., *Flight-Vehicle Materials, Structures, and Dynamics—Assessment and Future Directions*, Vol. 5, American Society of Mechanical Engineers, New York, 1993, pp. 179–212.

[3] Dowell, E. H., Clark, R., Cox, D., Curtiss, H. C., Jr., Edwards, J. W., Hall, K. C., Peters, D. A., Scanlan, R., Simiu, E., Sisto, F., and Strganac, T. W., (eds.) *A Modern Course In Aeroelasticity*, 4th ed., Kluwer Academic, Boston, Jan. 2005.

[4] Breitbach, E., "Effects of Structural Non-Linearities on Aircraft Vibration and Flutter," AGARD, Rept. 665, Jan. 1978.

[5] Yang, Z. C., and Zhao, L. C., "Analysis of Limit Cycle Flutter of an Airfoil in Incompressible Flow," *Journal of Sound and Vibration*, Vol. 123, No. 1, 1988, pp. 1–13.

[6] Strganac, T. W., and Mook, D. T., "Numerical Model of Unsteady Subsonic Aeroelastic Behavior," *AIAA Journal*, Vol. 28, No. 5, May 1990, pp. 903–909.

[7] Eastep, F. E., and Olsen, J. J., "Transonic Flutter Analysis of a Rectangular Wing with Conventional Airfoil Sections," *AIAA Journal*, Vol. 18, No. 10, Oct. 1980, pp. 1159–1164.

[8] Edwards, J. W., Bennett, R. M., Whitlow, W., and Seidel, D. A., "Time-Marching Transonic Flutter Solutions Including Angle-of-Attack Effects," *Journal of Aircraft*, Vol. 20, No. 11, Nov. 1983, pp. 899–906.

[9] Mukhopadhyay, V., "Benchmark Active Control Technology Special Section, Part 1," *Journal of Guidance, Control, and Dynamics*, Vol. 23, No. 5, 2000, pp. 913–960.

[10] Mukhopadhyay, V., "Benchmark Active Control Technology Special Section, Part 2," *Journal of Guidance, Control, and Dynamics*, Vol. 23, No. 6, 2000, pp. 1093–1139.

[11] Mukhopadhyay, V., "Benchmark Active Control Technology Special Section, Part 3," *Journal of Guidance, Control, and Dynamics*, Vol. 24, No. 1, 2001, pp. 146–192.

[12] Strganac, T. W., Ko, J., and Thompson, D. E., "Identification and Control of Limit Cycle Oscillations in Aeroelastic Systems," *Journal of Guidance, Control, and Dynamics*, Vol. 23, No. 6, 2000, pp. 1127–1133.

[13] Vipperman, J. S., Clark, R. L., Conner, M. D., and Dowell, E. H., "Investigation of the Experimental Active Control of a Typical Section Airfoil Using a Trailing Edge Flap," *Journal of Aircraft*, Vol. 35, No. 2, 1998, pp. 224–229.

[14] Wazak, M., and Srinathkumar, S., "Design and Experimental Validation of a Flutter Suppression Controller for the Active Flexible Wing," NASA TM 4381, 1992.

[15] Ko, J., Strganac, T. W., and Kurdila, A. J., "Stability and Control of Structurally Nonlinear Aeroelastic System," *Journal of Guidance, Control, and Dynamics*, Vol. 21, No. 5, 1998, pp. 718–725.

[16] Mukhopadhyay, V., "Flutter Suppression Digital Control Law Design and Testing for the AFW Wind Tunnel Model," NASA TM 107652, 1992.

[17] Ko, J., Kurdila, A. J., and Strganac, T. W., "Nonlinear Control of a Prototypical Wing Section with Torsional Nonlinearity," *Journal of Guidance, Control, and Dynamics*, Vol. 20, No. 6, 1997, pp. 1181–1189.

[18] Ko, J., Strganac, T. W., and Kurdila, A. J., "Stability and Control of Structurally Nonlinear Aeroelastic System," *Journal of Guidance, Control, and Dynamics*, Vol. 21, No. 5, 1998, pp. 718–725.

[19] Ko, J., Strganac, T. W., and Kurdila, A. J., "Adaptive Feedback Linearization for the Control of a Typical Wing Section With Structural Nonlinearity," *Nonlinear Dynamics*, Vol. 18, No. 3, 1999, pp. 289–301.

[20] Xing, W., and Singh, S. N., "Adaptive Output Feedback Control of a Nonlinear Aeroelastic Structure," *Journal of Guidance, Control, and Dynamics*, Vol. 23, No. 6, 2000, pp. 1109–1116.

[21] Strganac, T. W., Ko, J., and Thompson, D. E., "Identification and Control of Limit-Cycle Oscillations in Aeroelastic Systems," *Journal of Guidance, Control, and Dynamics*, Vol. 23, No. 6, 2000, pp. 1127–1133.

[22] Zhang, R., and Singh, S. N., "Adaptive Output Feedback Control of an Aeroelastic System with Unstructured Uncertainties," *Journal of Guidance, Control, and Dynamics*, Vol. 24, No. 3, 2001, pp. 502–509.

[23] Behal, A., Marzocca, P., Rao, V. M., and Gnann, A., "Nonlinear Adaptive Control of an Aeroelastic 2-D Lifting Surface," *Journal of Guidance, Control, and Dynamics*, Vol. 29, No. 2, Mar.–Apr. 2006, pp. 382–390.

[24] Platanitis, G., and Strganac, T. W., "Control of a Nonlinear Wing Section Using Leading- and Trailing-Edge Surfaces," *Journal of Guidance, Control, and Dynamics*, Vol. 27, No. 1, 2004, pp. 52–58.

[25] Behal, A., Rao, V. M., Marzocca, P., and Kamaludeen, M., "Adaptive Control for a Nonlinear Wing Section with Multiple Flaps," *Journal of Guidance, Control, and Dynamics*, Vol. 29, No. 3, May–June 2006, pp. 744–749.

[26] Tao, G., *Adaptive Control Design and Analysis*, Wiley, New York, 2003, pp. 458–472.
[27] Gujjula, S., Singh, S. N., and Yim, W., "Adaptive and Neural Control of a Wing Section Using Leading- and Trailing-Edge Surfaces," *Aerospace Science and Technology*, Vol. 9, No. 2, Mar. 2005, pp. 161–171.
[28] Block, J. J., and Strganac, T. W., "Applied Active Control for a Nonlinear Aeroelastic Structure," *Journal of Guidance, Control, and Dynamics*, Vol. 21, No. 6, 1998, pp. 838–845.
[29] O'Neil, T., "Experimental and Analytical Investigations of an Aeroelastic Structure with Continuous Nonlinear Stiffness," M. S. Thesis, Texas A&M University, College Station, TX, May 1996.
[30] Morse, A. S., "A Gain Matrix Decomposition and Some of its Applications," *Systems and Control Letters*, Vol. 21, No. 1, 1993, pp. 1–10.
[31] Krstić, M., Kanellakopoulos, I., and Kokotović, P., *Nonlinear and Adaptive Control Design*, Wiley, New York, 1995.
[32] Kokotovic, P., "The Joy of Feedback: Nonlinear and Adaptive," *IEEE Control Systems Magazine*, Vol. 12, 1992, pp. 7–17.
[33] Khalil, H., *Nonlinear Systems*, 3rd. ed., Prentice–Hall, Upper Saddle River, NJ, 1996.